Arabian Journal of Chemistry (2016) xxx, xxx–xxx

King Saud University

Arabian Journal of Chemistry

www.ksu.edu.sa
www.sciencedirect.com

ORIGINAL ARTICLE

Topochemical reduction of the oxygen-deficient Ruddlesden–Popper phase ($n = 1$) $La_{1.85}Ca_{0.15}CuO_{4-\delta}$ and electrical properties of the $La_{1.85}Ca_{0.15}CuO_{3.5}$

Adnene Midouni [a,e], **Mohamed Ikbal Houchati** [a,b,c,*], **Walid Ben Haj Othmen** [e], **Nassira Chniba-Boudjada** [d], **Ahmed Hichem Hamzaoui** [a]

[a] *Useful Materials Valorization Laboratory, National Centre of Research in Materials Science, Technologic Park of Borj Cedria, B.P. 73, 8027 Soliman, Tunisia*
[b] *Unité de Recherche Catalyse et Matériaux pour l'Environnement et les Procédés URCMEP (UR11ES85), Faculté des Sciences de Gabès/Université de Gabès, Campus Universitaire Cité Erriadh, Gabès 6072, Tunisia*
[c] *Institut de Chimie Moléculaire et des Matériaux-UMR 5253, C2M: Chimie et Crystallochimie des Matériaux, Université deMontpellier 2, 5 Place Eugène Bataillon, Bat 15, CC1504, F-34095 Montpellier, France*
[d] *Laboratoire de Cristallographie, CNRS, 25 Avenue des Martyrs, BP 166, 3804 Grenoble Cedex 9, France*
[e] *Laboratoire de Physico-Chimie des Matériaux Minéraux et leurs Applications, CNRSM, technopole de Borj Cedria, B.P. 95, Hammam-Lif 2050, Tunisia*

Received 24 March 2016; accepted 9 June 2016

KEYWORDS

Non-stoichiometric oxides;
Reduction via hydride method;
Oxygen mobility;
Electron paramagnetic resonance;
Electrical properties

Abstract The present paper reports on the synthesis, structure and electrical properties of the $La_{1.85}Ca_{0.15}CuO_{3.5}$ compound. The topotactic reduction of the tetragonal oxide T-$La_{1.85}Ca_{0.15}CuO_{4-\delta}$ with CaH_2 results in the formation of $La_{1.85}Ca_{0.15}CuO_{3.5}$. The powder X-ray diffraction data have shown that $La_{1.85}Ca_{0.15}CuO_{3.5}$ adopts a face-centered monoclinic crystal structure (A 2/m, $a = 8.6224(6)$, $b = 3.8446(2)$ Å, $c = 13.0179(10)$ and $\beta = 109.690(5)°$) with anion vacancies located within the CuO_2 ($CuO_{1.5}\square_{0.5}$, where $\square$ represents an anion vacancy) layer of the phase. The topotactic reduction of the complex transition metal $La_{1.85}Ca_{0.15}CuO_{4-\delta}$ may lead to the preparation of novel anion-deficient phases with unique transition metal-oxygen sublattices which cannot be prepared via the reduction of all-oxide substrates. The structural and chemical selectivity of the reduction process by anion de-intercalation and oxidation by anion insertion

* Corresponding author at: Useful Materials Valorization Laboratory, National Centre of Research in Materials Science, Technologic Park of Borj Cedria, B.P. 73, 8027 Soliman, Tunisia. Fax: +216 76 220 280.
E-mail address: ikb_med@yahoo.fr (M.I. Houchati).

Peer review under responsibility of King Saud University.

Production and hosting by Elsevier

http://dx.doi.org/10.1016/j.arabjc.2016.06.006

Please cite this article in press as: Midouni, A. et al., Topochemical reduction of the oxygen-deficient Ruddlesden–Popper phase ($n = 1$) $La_{1.85}Ca_{0.15}CuO_{4-\delta}$ and electrical properties of the $La_{1.85}Ca_{0.15}CuO_{3.5}$. Arabian Journal of Chemistry (2016), http://dx.doi.org/10.1016/j.arabjc.2016.06.006

are reviewed. The oxidative monoclinic ($La_{1.85}Ca_{0.15}CuO_{3.5}$) to tetragonal (T′-$La_{1.85}Ca_{0.15}CuO_{4-\delta}$) transition occurs at 380 °C. The structural determination combined with accurate compositional and electrical characterization indicates a change in the charge-compensating mechanism with phase transition.

1. Introduction

Transition metal oxides have always been the interest of scientists in many fields due to their various physical properties, such as superconductivity, magnetoresistance, and wealth of cooperative magnetic and transport behaviors. Such properties are strictly associated with the valence, coordination of transition metal centers and spin state, and how they are linked to form an extended network. Introducing many anion vacancies into transition metal oxides allows the tuning of these physical properties by changing the oxidation state and local coordination of transition metal centers. Besides, the presence of several vacant anion sites may bring about good ionic conductivity, offering these phases applications as fuel cell electrodes and membranes. The efficacy of ionic transport in anion-deficient systems has been proven to be intensely affected by the degree of order or disorder in the anion vacancy lattice. The prospective significance of these applications is the impetus behind the study of anion-deficient materials to examine the factors that control this ordering behavior in order to achieve better property optimizations (Mohn et al., 2009; Stolen et al., 2005).

The use of hydrides of electropositive metals as potent reducing agents such as NaH, LiH and CaH_2 at low-temperature, which is a technique recently introduced by Hayward, Rosseinsky, Dixon, Tsujimoto, Tassel, Romero and co-workers (Hayward et al., 1999; Hayward, 2005, 2006; Hayward and Rosseinsky, 2000; Dixon et al., 2011; Poltavets et al., 2006; Tsujimoto et al., 2007; Tassel et al., 2013; Seddon et al., 2010; Dixon and Hayward, 2011; Tassel et al., 2008, 2009; Yamamoto et al., 2010; Kageyama et al., 2008), has provided a way to avoid this structural choice. For example, using NaH, $YBaCo_2O_{4.5}$ and $LaBaCo_2O_{4.25}$ are synthesized from $YBaCo_2O_5$ and $LaBaCo_2O_5$, respectively (Seddon et al., 2010). Using the same reducing agent, NaH, $La_{1-x}Ca_xMnO_2$ is synthesized from $La_{1-x}Ca_xMnO_3$ ($0.6 \leqslant x \leqslant 1$) Dixon et al., 2011 and $LaNiO_2$ from $LaNiO_3$ (Hayward et al., 1999). Besides, using CaH_2, $La_3Ni_2O_6$ is synthesized from $La_3Ni_2O_7$ (Poltavets et al., 2006). Furthermore, a homologous series of $Sr_{n+1}Fe_n^{2+}O_{2n+1}$ ($n = 1$ Tassel et al., 2013, $n = 2$ (Kageyama et al., 2008) and $n = \infty$ (Tsujimoto et al., 2007) is obtained by CaH_2 from $Sr_{n+1}Fe_n^{4+}O_{3n+1}$. Moreover, using LiH, $Sr_3Fe_{2-x}Co_xO_4Cl_2$ is synthesized from $Sr_3Fe_{2-x}Co_xO_5Cl_2$ ($x = 0.2, 0.6, 0.8, 1$) (Dixon and Hayward, 2011).

Applying the new method to the T-phase $La_{1.85}Ca_{0.15}CuO_{4-\delta}$ Fig. 1a), we have recently obtained a new compound $La_{1.85}Ca_{0.15}CuO_{3.5}$ which has an unusual square-planar coordination around copper (Fig. 1b). This new phase is isostructural with $Nd_4Cu_2O_7$ (Pederzolli and Attfield, 1998), $La_2CuO_{3.5}$ (Houchati et al., 2012), $La_{1.5}Nd_{0.5}CuO_{3.5}$ (Houchati et al., 2012) and $La_{1.8}Pr_{0.2}CuO_{3.5}$ (Houchati et al., 2014). The oxidation of this phase in oxygen atmosphere below 380 °C leads to the formation of the T′-phase $La_{1.85}Ca_{0.15}CuO_{4-\delta}$ (Fig. 1c). This paper describes the structural transformation via a topotactic route reduction with a moderate temperature (The reaction mechanism for this T → pseudo-S → T′ phase sequence) of the $La_{1.85}Ca_{0.15}CuO_{4-\delta}$ phase to increase the concentration of oxygen vacancies in this complex 3d transition metal oxide. The main objective of this investigation was to determine the influence of the phase transition (pseudo S → T′) on the electrical conductivity (conduction mechanism) of the $La_{1.85}Ca_{0.15}CuO_{3.5}$ compound.

2. Experimental section

A powder sample of $La_{1.85}Ca_{0.15}CuO_{3.5}$ was synthesized by the hydride reaction of a slightly oxygen-deficient $La_{1.85}Ca_{0.15}CuO_{4-\delta}$ ($\delta \sim 0.09$) with CaH_2. By the use of a solid-state ceramic route, five grams of $La_{1.85}Ca_{0.15}CuO_{4-\delta}$ precursor was prepared from predried CuO (99.99%), CaO (99.99%) and La_2O_3 (99.99%), which had been previously dried at 1173 K for 12 h prior being weighed to decompose eventual traces of lanthanum hydroxide. After mixing in the appropriate ratio, the mixture was heated in air at 1173 K for 24 h. The resulting black powder was then reground and pressed into pellets (1 g in weight, 13 mm diameter) with a force of 8 tons which were sintered at 1273 K for 48 h in air with one intermediate pressing and grinding step. For reduction, $La_{1.85}Ca_{0.15}CuO_{4-\delta}$ (1 g) and a two-molar excess of CaH_2 (0.5 g) were mixed, finely ground and pelletizing in an N_2-filled glove box (O_2 and H_2O levels < 1 ppm). The pellet was then sealed in an evacuated Pyrex tube (23 cm in length and 2 cm in diameter), and heated in a muffle furnace at 553 K for two days. The resulting mixture contained a new phase, unreacted CaH_2 and byproducts such as CaO according to XRD analysis. The reaction product was then washed with 0.1 M NH_4Cl/CH_3OH solution in air to remove the excess of CaH_2 and CaO, and dried in a vacuum oven at 383 K.

2.1. Characterization techniques

The sample purity was checked by X-ray powder diffraction (XRD) (these data were also used for the structure characterization) at room temperature using a PANalytical X'Pert diffractometer equipped with a Cu Kα source ($\lambda = 1.5406$ Å). Data were collected over a 2θ range of 10–120° for Rietveld refinement.

The nuclear structures were determined by neutron diffraction on the D1A diffractometer ($\lambda = 1.91$ Å), at the ILL Grenoble. Powder data were refined with the FullProf refinement Package. A polycrystalline sample of $1-g$ mass was placed into a vanadium cylinder. The Data were collected with step-scan procedure in a 2θ range from 0° to 160° with a final step width of 0.05°.

The crystal structure and cell parameters were refined by the Rietveld method (Rietveld, 1969; McCusker et al., 1999) using the FullProf program (Rodríguez-Carvajal, 1993). The peak shape model used was a modified split-pseudo-Voigt function. The agreement indices used were R-weighted pattern factor, $R_{wp} = [\Sigma wi(yio - yic)^2/\Sigma w_i(y_{io})^2]^{1/2}$, R-pattern, $R_p = \Sigma|y_{io} - y_{ic}|/\Sigma(y_{io})$, R-Bragg factor, $R_I = \Sigma|I_o(h_k) - I(h_k)|/\Sigma I_o(h_k)$ and goodness of fit (GOF), $\chi^2 = [R_{wp}/R_{exp}]^2$, where $R_{exp} = [(N - P)/\Sigma w_i y_{io}^2]^{1/2}$, y_{io} and y_{ic} are the observed and calculated intensities, w_i is the weighting factor, $I_o(h_k)$ and

Please cite this article in press as: Midouni, A. et al., Topochemical reduction of the oxygen-deficient Ruddlesden–Popper phase ($n = 1$) $La_{1.85}Ca_{0.15}CuO_{4-\delta}$ and electrical properties of the $La_{1.85}Ca_{0.15}CuO_{3.5}$. Arabian Journal of Chemistry (2016), http://dx.doi.org/10.1016/j.arabjc.2016.06.006

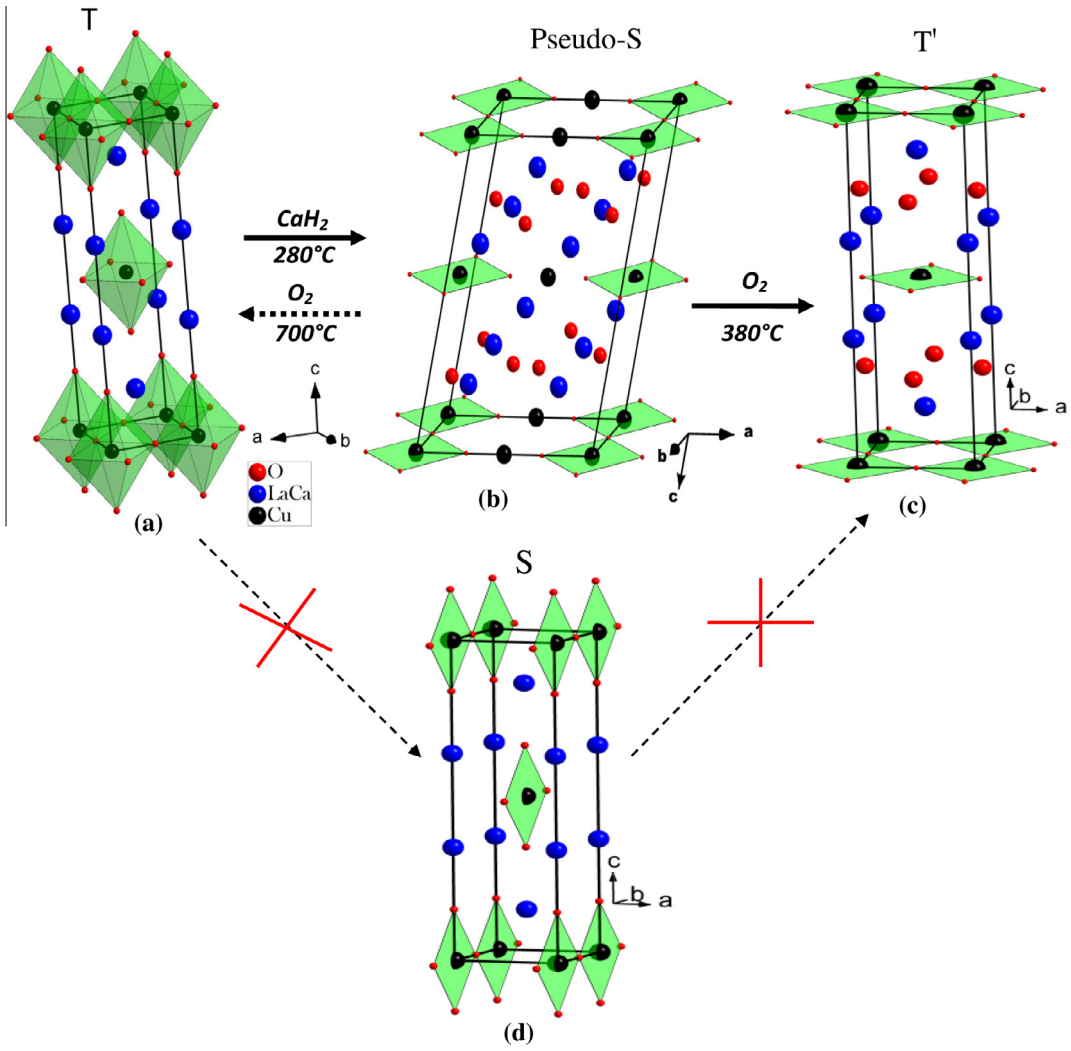

Figure 1 Topochemical reduction of $La_{1.85}Ca_{0.15}CuO_{4-\delta}$ occurs in association with a rearrangement of the anion lattice to yield $La_{1.85}Ca_{0.15}CuO_{3.5}$, a phase containing square-planar $Cu^{(I/III)}O_4$ units ((a) $La_{1.85}Ca_{0.15}CuO_{4-\delta}$ with the K_2NiF_4-type (T), (b) structure models of $La_{1.85}Ca_{0.15}CuO_{3.5}$, (c) $La_{1.85}Ca_{0.15}CuO_4$ with the Nd_2CuO_4-type (T′) structure, and (d) $La_{1.85}Ca_{0.15}CuO_{3.5}$ with the Sr_2CuO_3-type (S) structure).

$I(h_k)$ are the observed and calculated integrated intensities, N is the total number of y_{io} data when the background is refined, and P is the number of adjusted parameters. B_{iso} is the isotropic temperature factor.

Metler Toldo DSC823e Differential Scanning Calorimeter (DSC) was used to examine the phase behavior of the compound. The DSC scans were recorded using 5 mg of the sample which were powdered in order to determine, to establish or rule out the possible existence of phase transitions in the solid sample. The diagrams were obtained from temperature sweep experiments by heating the mixed system using platinum crucible from 323 to 923 K at the rate 10 K/min.

Electron Paramagnetic Resonance Spectroscopy (EPR) analysis was carried out with a Bruker ER-200D spectrometer having X-band frequencies (9.30 GHz). All spectra were recorded at the ambient temperature of the EPR laboratory. Cylindrical quartz sample tubes of 15 mm diameter were used for measurements.

The impedance spectroscopy was performed on pellet discs of about $d = 8$ mm diameter and a $e = 1.5$ mm thickness. Pt electrodes were fixed on the opposite faces of each pellet by applying a coating of silver paste to ensure good electrical contact. After the Ag coating and before measurements, the samples were first heated at 393 K for 12 h under vacuum. This treatment is carried out to eliminate, as much as possible, the water content in the pellet pores. The ac impedance data, $|Z|$ and phase angle were obtained in the frequency range of 40 Hz–5 MHz with the AGILENT 4294A Precision Impedance Analyzer monitored by a micro-computer between 323 and 973 K. The impedance data analysis and equivalent circuit fitting were carried out with Zview 2.8 software (ZView for Windows, xxxx) and Origin8.

The oxidation state of copper ions and oxygen content (assuming charge neutrality: La^{3+}, Ca^{2+}, O^{2-}) of samples were determined by iodometric titration technique performed argon flow (Krogh Andersen et al., 1994; Alyoshin et al.,

Please cite this article in press as: Midouni, A. et al., Topochemical reduction of the oxygen-deficient Ruddlesden–Popper phase ($n = 1$) $La_{1.85}Ca_{0.15}CuO_{4-\delta}$ and electrical properties of the $La_{1.85}Ca_{0.15}CuO_{3.5}$. Arabian Journal of Chemistry (2016), http://dx.doi.org/10.1016/j.arabjc.2016.06.006

2010). In order to determine the copper oxidation state, two powdered samples of nearly 0.08 g were taken. The first sample with mass m_1 was dissolved in HCl solution (37%) in the presence of an excess of potassium iodide KI. The formed iodine I_2 was rapidly titrated with a volume V_1 of sodium thiosulfate $Na_2S_2O_3$ standard solution added at the end point indicated by the colour change of the starch indicator.

$$Cu^{2+} + 2I^- = CuI \downarrow + 1/2I_2 \quad (1)$$

$$I_2 + 2Na_2S_2O_3 = 2NaI + Na_2S_2O_6 \quad (2)$$

The second sample with mass m_2 was dissolved under stirring in potassium iodide KI solution with addition of a small amount of diluted HCl.

$$Cu^{(2+\tau)+} + (2+\tau)I^- = CuI \downarrow + 1/2(1+\tau)I_2 \quad (3)$$

Likewise, the formed I_2 was also titrated with a volume V_2 of standard sodium thiosulfate solution. The average copper oxidation state V (Cu) and the oxygen vacancy concentration (deviation from stoichiometry) δ can be calculated according to the following equations:

$$V(Cu) = 2 + \tau; \tau = (V_2/m_2 - V_1/m_1)/(V_1/m_1) \quad (4)$$

$$\delta = [2 + x(Ca) - V(Cu)]/2 \quad (5)$$

The tests were carried out at least three times for each sample. The oxygen under-stoichiometry estimated by iodometric titration indicated that δ is equal to 0.0896(7) and 0.5243(5) for the compounds T-$La_{1.85}Ca_{0.15}CuO_{4-\delta}$ and "pseudo-S" $La_{1.85}Ca_{0.15}CuO_{3.5}$ respectively.

3. Results and discussions

3.1. Structural refinement of T-$La_{1.85}Ca_{0.15}CuO_{4-\delta}$

Fig. 2 shows the XRD patterns of the precursors $La_{2-x}Ca_xCuO_{4-\delta}$ for $x = 0$–0.15. The XRD profiles for $0 \leqslant x \leqslant 0.125$ are very similar to each other and readily indexed on the basis of the orthorhombic (space group *Bmab*) unit cell without any peaks associated with impurities or superreflections. However, the profile for $x = 0.15$ corresponding to the solubility limit of Ca^{2+} in La_2CuO_4 adopts a body-centered tetragonal crystal structure (space group *I*4/*mmm*). The aliovalent substitution of La^{3+} by Ca^{2+} given by eqs (6) and (7), the charge compensation mechanisms can be represented by two defect equations (using the Kröger-Vink notation) involving either vacancies in the anion substructure ($V_O^{\cdot\cdot}$) or hole ($h^{\cdot}$) formation (oxidation of Cu^{2+} to Cu^{3+}). The presence of oxygen vacancies and hole ($h^{\cdot}$) formation is relevant for understanding the electrical properties.

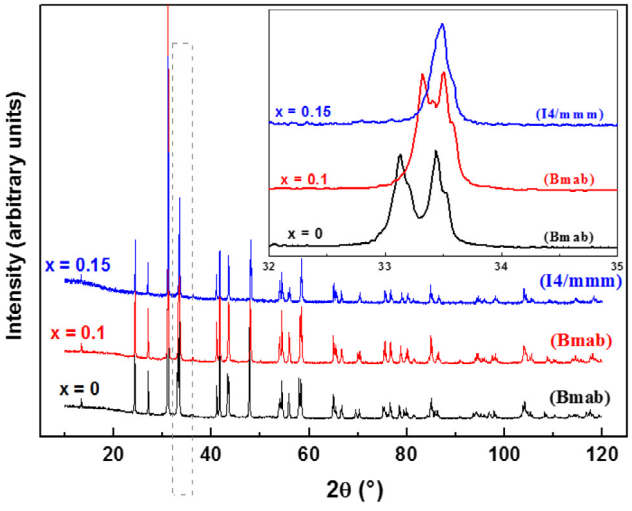

Figure 2 XRD patterns of $La_{2-x}Ca_xCuO_{4-\delta}$ (for $x = 0$, $\delta = 0$). All the patterns except $x = 0.15$ (tetragonal, space group *I*4/*mmm*) could be indexed on the basis of an orthorhombic (space group, *Bmab*) unit cell.

$$2\ CaO = 2Ca'_{La} + V_O^{\cdot\cdot} + 2\ O_O^X \quad (6)$$

$$2\ CaO + 2\ Cu_{Cu}^X + 1/2O_2 = 2Ca'_{La} + 2Cu_{Cu}^{\cdot} + 3O_O^X \quad (7)$$

The powder X-ray diffraction (XRD) patterns of the precursor phase $La_{1.85}Ca_{0.15}CuO_{4-\delta}$ indicated the formation of a single tetragonal $n = 1$ Ruddlesden-Popper, K_2NiF_4-like phase with no impurity phases, crystallize with body-centered tetragonal cell described by the ideal, high-symmetry space group *I*4/*mmm* as seen in the inset of Fig. 2 (The orthorhombic → tetragonal transition). From the Rietveld refinement, it was clear that a single phase material had successfully been produced through the ceramic method synthesis route. Fig. 1a shows the T-$La_{1.85}Ca_{0.15}CuO_{4-\delta}$ tetragonal unit-cell, the structure is strongly anisotropic, almost bi-dimensional since the thickness of perovskite layers is minimal; the octahedra share corners but are not interconnected between layers. The fact that $n = 1$ implies that each CuO_6 octahedral layer is sandwiched between two slabs of rock salt (La/Ca)O. La ions occupy a single site at the boundary between the two types of layers, corresponding to the A site of coordination number 9, i.e. 4 + 4 + 1 oxygen ions with different bond lengths. The Cu cations are in coordination 4 + 2 of equatorial (O_{eq}) and apical oxygen (O_{ap}) respectively. Refinements using the tetragonal symmetry *I*4/*mmm* model gave a good fit, providing reasonable reliability factors $R_{wp} = 7.71\%$, $R_p = 5.94\%$ and $\chi^2 = 1.6$ along with reasonable individual, isotropic displacement factors for all atoms, suggesting successful structural analysis. The values of the refined structural parameters and the interatomic distances are recorded in Tables. S1 and S2 respectively. The structural refinements readily converged with good agreement between observed and calculated diffraction patterns, as shown in Fig. S1.

3.2. Localization of oxygen vacancies in T-$La_{1.85}Ca_{0.15}CuO_{4-\delta}$

The PND technique was used for the localization of oxygen vacancies and determined the oxygen deviation from stoichiometry δ. The slightly oxygen-deficient phase T-$La_{1.85}Ca_{0.15}CuO_{4-\delta}$ was prepared for the neutron diffraction study; the PND pattern of T-$La_{1.85}Ca_{0.15}CuO_{4-\delta}$ is presented in Fig. 3. The structural data and goodness of fit parameters for the final refinement are listed in Table 1. The total oxygen contents of the T-$La_{1.85}Ca_{0.15}CuO_{4-\delta}$ sample were determined from PND data recorded at room temperature. These measurements allowed us to determine the occupancy factor of the oxygen crystallographic sites O_{eq}, O_{ap}, in the $n = 1$ RP phase crystal structure. Different structural

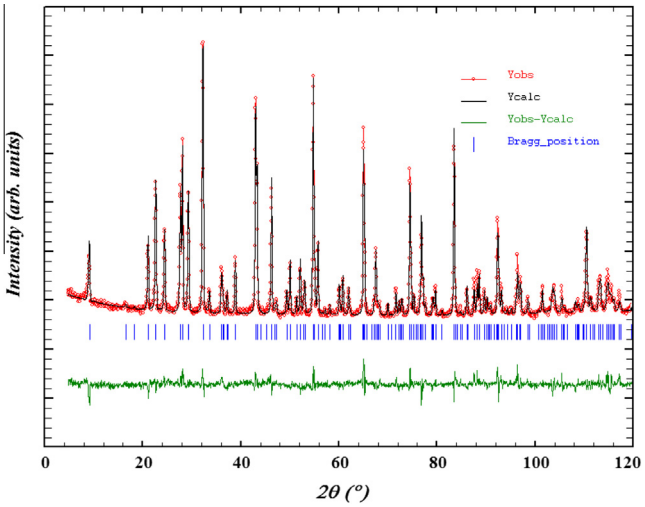

Figure 3 Rietveld refinement profiles for the PND data of $La_{1.85}Ca_{0.15}CuO_{4-\delta}$: observed intensities (crosses), calculated pattern (solid line), difference curve (bottom solid line), and Bragg positions (tick marks).

Table 1 Structure data of $La_{1.85}Ca_{0.15}CuO_{4-\delta}$ obtained from Rietveld refinement of neutron powder diffraction on D1A @ ILL Grenoble, (λ = 1.91 Å).

Atom	Site	x	y	z	B_{iso} (Å^2)	Occupancy
La/Ca	4e	0	0	0.3606(1)	0.7210(9)	1.85/0.15
Cu	2a	0	0	0	0.6550(3)	1
O_{eq}	4c	0	0.5	0	0. 9980(1)	2
O_{ap}	4e	0	0	0.1828(2)	1.5460(1)	1.9095

(O_{eq} = Equatorial oxygen, O_{ap} = Apical oxygen).
*I*4/*mmm*, Z = 2, a = 3.7784(1) Å, c = 13.1669(4) Å, V = 187.9830 (9) Å^3, R_{wp} = 5.68%, R_p = 4.31%, R_I = 2.88%, and χ^2 = 3.86.

models with localization of oxygen vacancies on 4e and/or 4c sites were tested for sample with x(Ca) = 0.15. The oxygen vacancies were detected unambiguously in {(La/Ca)O} layers (4e site). The concentration of oxygen vacancies in T-$La_{1.85}Ca_{0.15}CuO_{4-\delta}$ was found to be δ = 0.0905(6). The quality of the refinement decreases when the model assumes that both O_{ap} sites are fully occupied and oxygen vacancies are located only on the O_{eq} site. For example, the R_{wp} and χ^2 parameters increase their values from 5.63 and 3.79 to 6.03 and 4.35, respectively, if the O_{ap} site is considered fully occupied.

3.3. Structural refinement of $La_{1.85}Ca_{0.15}CuO_{3.5}$

X-ray powder diffraction data collected from the reduced $La_{1.85}Ca_{0.15}CuO_{3.5}$ sample could be readily indexed on the basis of A-centered monoclinic cell (space group *A*2/*m*) with the following lattice parameters: a = 8.6198(2) Å, b = 3.8433 (7) Å, c = 13.0136(8) and = 109.684(2)°. Structural model based on the refined structure of $La_{1.85}Ca_{0.15}CuO_{3.5}$ is similar to those found from $Nd_4Cu_2O_7$ (Pederzolli and Attfield, 1998), $La_{1.5}Nd_{0.5}CuO_{3.5}$ (Houchati et al., 2012) and $La_{1.8}Pr_{0.2}CuO_{3.5}$ (Houchati et al., 2014). Traces of $La(OH)_3$ Houchati et al., 2012, 2014 were detected in $La_{1.85}Ca_{0.15}CuO_{3.5}$ sample, which was included in these refinements as a second phase. However, the $La(OH)_3$ content was in the order of 2% (relative to the sample weight), and thus it is considered to have a negligible effect on the stoichiometry of the material. The concentration of oxygen vacancies in $La_{1.85}Ca_{0.15}CuO_{3.5}$ (δ = 0.5), is in good agreement with the results obtained by iodometric titration δ = 0.5243(5). The structure of $La_{1.85}Ca_{0.15}CuO_{3.5}$ is derived from that of Nd_2CuO_4 by the ordered removal of one-quarter of the oxygen atoms in the CuO_2 layers, as indicated in Fig. 1b. This gives rise to seven-coordinated La/Ca sites and alternating fourfold and twofold coordinated Cu sites along the a-axis. The structure of $La_{1.85}Ca_{0.15}CuO_{3.5}$, formally consisting of mixed-valent Cu^{1+}/Cu^{3+} species, shows two different copper sites, Cu(1) in a 4-fold planar coordination with two short (1.9223(10) Å) and two longer (2.2520(4) Å) Cu−O distances, while Cu(2) has a linear twofold coordination with Cu−O distance of 2.0711 (5) Å. The (La/Ca)O_9 polyhedron in the K_2NiF_4-type framework gets reduced to two symmetrically nonequivalent but nevertheless similar (La/Ca)O_7 polyhedra for $La_{1.85}Ca_{0.15}CuO_{3.5}$, with bonding distances ranging from 2.3205(9) to 2.7939(2) Å (see Table 3). A structural description of this phase was added to the refinement model, which readily converged to give a good statistical fit to the data (χ^2 = 2.12). Full details of the refined structural parameters are presented in Table 2, with selected bond lengths in Table 3. A Plot of the observed against calculated diffraction data is shown in Fig. 4. On the other hand T-$La_{1.85}Ca_{0.15}CuO_{4-\delta}$ can be transformed into T′-$La_{1.85}Ca_{0.15}CuO_{4-\delta}$ via a two-step topotactic reaction mechanism. First T-$La_{1.85}Ca_{0.15}CuO_{4-\delta}$ is reduced by CaH_2 at 553 K to $La_{1.85}Ca_{0.15}CuO_{3.5}$ which can be subsequently reoxidized to T′-$La_{1.85}Ca_{0.15}CuO_{4-\delta}$ at 653 K in air. $La_{1.85}Ca_{0.15}CuO_{3.5}$ does not adopt the Sr_2CuO_3 type "S-phase" structure, as taken for granted for almost 20 years, but constitutes an oxygen deficient T′-framework, with copper in 4-fold planar and 2-fold linear dumbbell coordination. Upon heating the T-$La_{1.85}Ca_{0.15}CuO_{4-\delta}$ phase is reobtained from T′-$La_{1.85}Ca_{0.15}CuO_{4-\delta}$ above 923 K, confirming the "T-phase" to be the thermodynamically stable modification at least at higher temperature. Sr_2CuO_3-type (S) structure can be indexed with an I-centered orthorhombic lattice with $a \sim 3.55$ Å,

Table 2 Atomic coordinates, occupancies, and isotropic temperature factor obtained by Rietveld refinement of X-ray powder diffraction data for $La_{1.85}Ca_{0.15}CuO_{3.5}$.

Atom	x	y	z	B_{iso} (Å^2)	Occupancy
La_1/Ca_1	0.1746(5)	0	0.3446(3)	0.8732(1)	1.85/0.15
La_2/Ca_2	0.3150(6)	0.5	0.1463(6)	0.5324(6)	1.85/0.15
Cu_1	0	0	0	0. 9476(3)	1
Cu_2	0.5	0	0	0.7519(5)	1
O_1	0	0.5	0	1.2132(3)	1
O_2	0.2289(6)	0	0.0271(1)	0.7953(1)	2
O_3	0.3186(7)	0	0.8356(6)	0. 6731(4)	2
O_4	0.3650(6)	0	0.2593(2)	1.1318(6)	2

Space group *A*2/*m* (12): a = 8.6198(2) Å, b = 3.8433(7) Å, c = 13.0136(8), β = 109.684(2)°, V = 406.3069 Å^3, Z = 2, R_{wp} = 3.78%, R_p = 2.92%, R_I = 2.778%, and χ^2 = 2.12.

Table 3 Selected bond lengths obtained from Rietveld refinements performed against X-ray powder diffraction data for $La_{1.85}Ca_{0.15}CuO_{3.5}$.

Bond	Bond length (Å)
(La_1/Ca_1)–O_1 (x1)	2.7939(2)
(La_1/Ca_1)–O_2 (x2)	2.7101(3)
(La_1/Ca_1)–O_3 (x1)	2.3978(6)
(La_1/Ca_1)–O'_3 (x2)	2.3205(9)
(La_1/Ca_1)–O_4 (x1)	2.6071(16)
(La_2/Ca_2)–O_1 (x1)	2.7362(2)
(La_2/Ca_2)–O_2 (x2)	2.5901(3)
(La_2/Ca_2)–O_3 (x1)	2.2279(17)
(La_2/Ca_2)–O_4 (x2)	2.2932(10)
(La_2/Ca_2)–O'_4 (x1)	2.4849(19)
Cu_1–O_1 (x2)	1.9223(10)
Cu_1–O_2 (x2)	2.2520(4)
Cu_2–O_2 (x2)	2.0711(5)

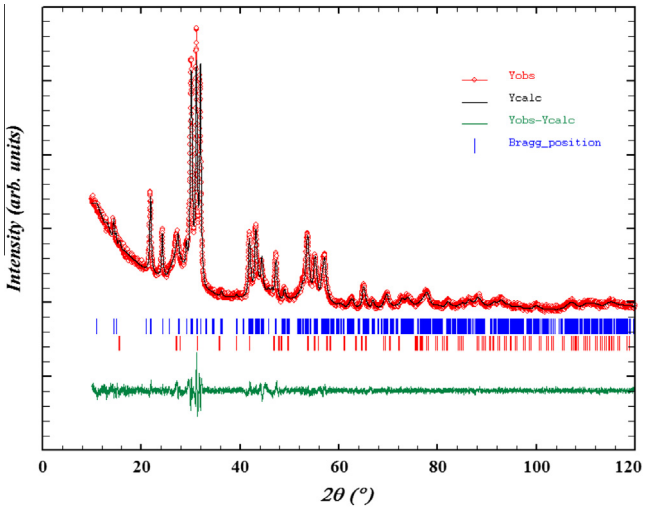

Figure 4 Structural characterization of $La_{1.85}Ca_{0.15}CuO_{3.5}$ by Rietveld refinement of X-ray powder diffraction (XRD) at RT. Dotted line (red), solid lines (black), and blue solid line stand for the observed, calculated, and difference intensities, respectively. Green ticks indicate the position of the calculated Bragg reflections of, from up to down, $La_{1.85}Ca_{0.15}CuO_{3.5}$ and $La(OH)_3$.

$b \sim 3.93$ Å, and $c \sim 12.95$ Å. This structure is composed of chains of corner-linked square planar CuO_4 units separated by parallel chains of ordered vacancies (see Fig. 1d). The reaction pathway from T → T′ does not proceed via the T → S → T′ phase sequence (Chou et al., 1990), but implies the formation of a "pseudo-S" $La_{1.85}Ca_{0.15}CuO_{3.5}$ oxygen vacancy ordered intermediate phase with monoclinic symmetry.

3.4. Structural Refinement of T′-$La_{1.85}Ca_{0.15}CuO_{4-\delta}$

The structure of the type T′-$La_{1.85}Ca_{0.15}CuO_{4-\delta}$ is derived from that of the type T-$La_{1.85}Ca_{0.15}CuO_{4-\delta}$ by a topotactic reduction–oxidation through the intermediate "pseudo S" $La_{1.85}Ca_{0.15}CuO_{3.5}$ phase. Conceptually, the process consists of taking off oxygen atoms from the structure, creating vacancies and oxygen disorder, then re-introducing oxygen at relatively low temperature, yielding stabilization of T′ instead of T-type structure. To achieve this conversion, two steps have been performed: First T-$La_{1.85}Ca_{0.15}CuO_{4-\delta}$ is reduced by CaH_2 at 280 °C to $La_{1.85}Ca_{0.15}CuO_{3.5}$ which can be subsequently reoxidized to T′-$La_{1.85}Ca_{0.15}CuO_{4-\delta}$ at 380 °C in air according to the following chemical reaction:

$$La_{1.85}Ca_{0.15}CuO_{3.5} + 1/4O_{2-4\delta} = T' - La_{1.85}Ca_{0.15}CuO_{4-\delta} \quad (8)$$

The basic structural difference between T and T′ consists only in one oxygen position in the unit-cell. In T′ structure, the apical site is empty whereas interstitial site is completely full and vice versa for T-structure. The structures of the T and the T′-type phases can be described as the intergrowth of perovskite and rock-salt (in T) and infinite layer and fluorite (in T′-type) structural blocks. The formation of the T′ from T phase occurs as a result of an oxygen deintercalation and a structural rearrangement in the (La/Ca)O part of the structure. The oxygen atoms from the (La/Ca)O layers in the perovskite blocks of the T phase are completely removed during the reduction process.

Instead of occupying this site, oxygen ions are located in the interstitial planes ($z = 0.25$ and $z = 0.75$). Therefore, copper layers consisted of planar array of corner-shared CuO_4 square planes, thus forming infinite CuO_2 layers. The coordination number of Cu is 4 instead of 6 for the T-phase, and that of La is 8 instead of 9. The absence of apical oxygen occurring for CuO_6 octahedra leads to structural frustrations induced by the Jahn-Teller effect. Interestingly, in the case of $La_{1.85}Ca_{0.15}(Cu_{1-x}Ni_x)O_{4-\delta}$ ($x = 0.0$, 0.1, 0.2 and 0.3) series, display significant Jahn-Teller (JT) distortions of the Cu(Ni)O_6 site cations. The coordination polyhedra of Cu(Ni) are distorted octahedra, which are contracted for x(Ni) = 0.2 and 0.3 and elongated for x(Ni) = 0.1, compared with x(Ni) = 0.0, in the axial direction due to the JT effect (d^9 configuration of Cu^{2+}), as confirmed by the bond distances obtained from XRD refinements. The degree of distortion Δ_{JT} is given by the apical bond length divided by the equatorial bond length (Δ_{JT} = d(Cu(Ni)–O_{ap}/d(Cu(Ni)–O_{eq})) Bouloux et al., 1981. This distortion decreases linearly with the content of Ni (Midouni et al., 2016). In addition, $CuWO_4$ phase has a transition on the basis of SXRD, and the transition is from the triclinic (P1) structure to a monoclinic (P2/c) structure. The transition implies abrupt changes of CuO_6 and WO_6 octahedra, but no coordination change. Further, we report the role played by the Jahn Teller distortion of the CuO_6 octahedra on the mechanism of the phase transition as well as the changes in the behavior of the Cu–O bonds for the triclinic and monoclinic phases of $CuWO_4$. We can say, in spite of the six different Cu–O bond distances, the CuO_6 units can be considered as elongated octahedra with four short and two longer bonds (Ruiz-Fuertes et al., 2011).

The value of c-parameter of 13.1728(3) Å for T-phase is higher than that of the T′ unit-cell corresponding to the value of 12.5428(3) Å. Conversely, the a-parameter increases to 3.9885(6) Å instead of 3.7784(1) Å for T-phase. The volume of the T′unit-cell (199.5390(7) $Å^3$) is larger than that of T-unit-cell (188.3746(2) $Å^3$). It should be noted that the T′-$La_{1.85}Ca_{0.15}CuO_{4-\delta}$ structures do not allow oxygen vacancies despite their preparation by oxygen deintercalation. The refined structural data for T′-$La_{1.85}Ca_{0.15}CuO_{4-\delta}$ and

Table 4 Atomic coordinates, occupancies, isotropic temperature factor and bond lengths obtained by Rietveld refinement of X-ray powder diffraction data for T′-$La_{1.85}Ca_{0.15}CuO_4$.

Atom	Site	x	y	z	B_{iso} (Å^2)	Occupancy
La/Ca	4e	0	0	0.3279(8)	1.29(5)	1.85/0.15
Cu	2a	0	0	0	1.09(4)	1
O_1	4c	0	0.5	0	3.54(2)	2
O_2	4d	0	0.5	0.25	2.73(9)	2
Bond length (Å)						
Cu–O_1 (x4): 1.9761(7)						
(La/Ca)–O_2 (x4): 2.3325(4)						

Space group *I*4/*mmm* (139): a = 3.9885(6) Å, c = 12.5428(3) Å, V = 199.5390 Å^3, Z = 2, R_{wp} = 10.71%, R_p = 8.94%, R_I = 7.3% and χ^2 = 9.68.

goodness of fit parameters are summarized in Table 4, and the experimental and calculated spectra as well as the difference between them are shown in Fig. 5.

The fact that $La_{1.85}Ca_{0.15}CuO_{3.5}$ does not adopt the "S-type" structure, as taken for granted for more than 20 years, but an oxygen deficient T′-framework, must be considered as a chance from a synthetic point of view, implying the possibility to transform K_2NiF_4 type oxides other than $La_{1.85}Ca_{0.15}CuO_4$ toward the T′-framework. This concerns especially the synthesis of defined electron doped T′-$La_{2-x}RE_xCuO_4$ (RE = Ce...) compounds, which are not accessible through the molten salt synthesis, and which are complementary to the hole doped T-$La_{2-x}Sr_xCuO_4$ or T-$La_2CuO_{4+\delta}$, allowing us to cross-check their superconducting properties for respective symmetrical doping levels. The Sr_2CuO_3 structure type can, however, at this stage, no longer be extended to the $La_2CuO_{4-\delta}$ system. It still is, as long as oxides are concerned, limited to a few phases only, e.g., $(Ca/Sr/Ba)_2CuO_3$ Teske and Müller-Buschbaum, 1969a,b; Wong-Ng et al., 1988 as well as $(Sr/Ba)_2PdO_3$ Wasel-Nielen and Hoppe, 1970; Laligant et al., 1988.

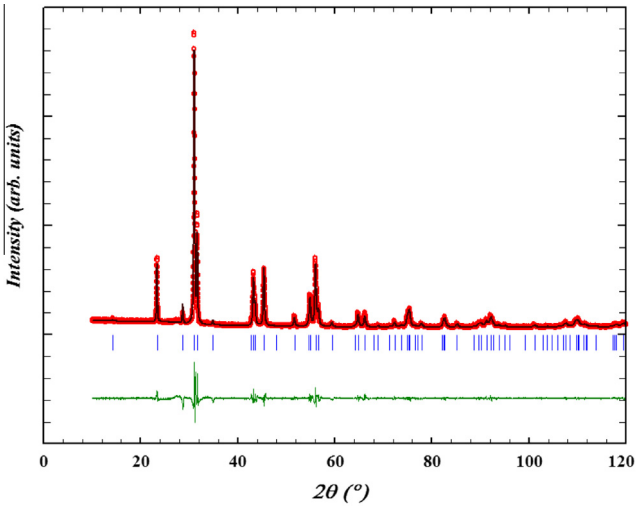

Figure 5 Rietveld refinement profiles for the XRPD data of T′-$La_{1.85}Ca_{0.15}CuO_4$: observed intensities (dotted line, red), calculated pattern (solid line, black), difference curve (bottom solid line, blue), and Bragg positions (tick marks, green).

3.5. Calorimetric studies

The transition from T to T′ phase (Houchati et al., 2014) undergone by the $La_{1.85}Ca_{0.15}CuO_{4-\delta}$ compound involves a primary transformation via one intermediate phase, stable in a narrow range of temperature (653 K). In order to measure precisely the temperatures of the transitions, Differential Scanning Calorimetry (DSC) experiments were performed. The DSC thermogram was recorded for the $La_{1.85}Ca_{0.15}CuO_{3.5}$ sample heated in an oxygen flow of 20 cm^3/min as the temperature increased from 323 to 923 K at a rate of 10 K/min and depicted in Fig. S2 of ESI. The thermogram reveals one peak endothermic at 650 K. He can be attributed to the oxidation of the $La_{1.85}Ca_{0.15}CuO_{3.5}$ phase, which implies an increase in oxygen. This transition at 650 K can be accredited to the transition of the "pseudo-S" phase to the T′-$La_{1.85}Ca_{0.15}CuO_{4-\delta}$ phase. Such tentative of attributions is confirmed by X-ray diffraction studies. The confirmation of the phase transition from DSC was also obtained by Trigui et al. for the $[(C_4H_9)_4N]_3Bi_2Cl_9$ compound (Trigui et al., 2015).

3.6. Electron paramagnetic resonance (EPR)

Fig. 6a shows that the compound before reduction, $La_{1.85}Ca_{0.15}CuO_{4-\delta}$ is non-paramagnetic, which is explained by the absence of characteristic signals is concerned and hence we do not discuss the parent phase system further. Contrariwise, for the case of the $La_{1.85}Ca_{0.15}CuO_{3.5}$ (after reduction) system, we observed a drastic change in the EPR signals. For this system, we note the presence a characteristic 8-fold structure (marked by arrows in Fig. 6b), with the g-values in the range 2.024–2.367. From the structural details on the $La_{1.85}Ca_{0.15}CuO_{3.5}$ unit cell, we have the Cu_1^{2+} centers in a distorted square plane; in fact, the signal form indicates the symmetry of the site, where the single electron is found. Further, La^{3+} and Ca^{2+} ions are non-paramagnetic and also their nuclear spins are too low to account for the 8-fold structure observed and hence the contributions from these ions can be discounted.

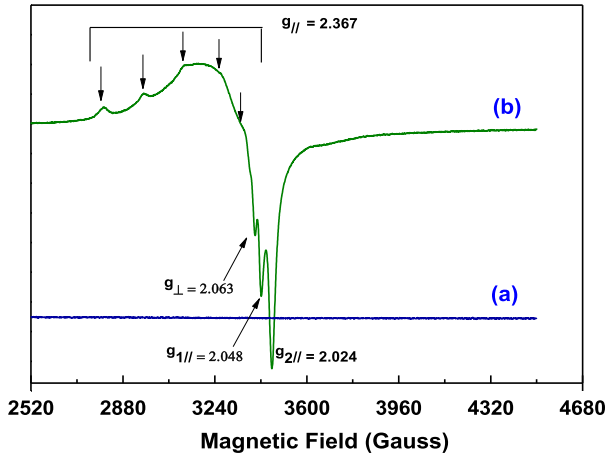

Figure 6 EPR spectra of (a) $La_{1.85}Ca_{0.15}CuO_{4-\delta}$ and (b) $La_{1.85}Ca_{0.15}CuO_{3.5}$ at RT.

The Cu^{2+} ion having d^9 electron configuration (with $S = \frac{1}{2}$ and $I = \frac{3}{2}$) works as though we have a hole in a filled d-shell. The *g*-values observed for the structure clearly reflect the involvement of holes and further the 8-fold structure observed could be assigned to the hyperfine structure from the two isotopes of Cu^{2+} (^{63}Cu and ^{65}Cu) Sai Sundar et al., 1999. This is consistent with the relation $2(2I + 1) = 8$ hfs (hfs: hyperfine structure) components observed. In all fairness, these observations enable us to propose that the hole centers are coupled with Cu^{2+} nuclei and hence are localized around Cu^{2+} centers. This observation is in agreement with the theoretical model of Pokrovsky and Uimin predicting localization of holes in the CuO_2 sheets of the Sr-doped La_2CuO_4 system (Pokrovsky and Uimin, 1989). The apparition of peaks in EPR spectrum of the reduced sample compared to the parent phase spectrum seems to be strongly correlated to the new oxygen distribution induced by the reduction process and especially the suppression of apical oxygen in the pseudo-S phase.

3.7. Electrical properties

The Nyquist plots of the $La_{1.85}Ca_{0.15}CuO_{3.5}$ compound presented at different temperatures are reported in Fig. 7. The plots are semicircle arcs centered below the real axis, showing that the impedance data follow the pattern of Cole–Cole model (Grimnes and Martinsen, 2005). As temperature increases, the radius of the arc corresponding to the bulk resistance of the sample decreases, indicating an activated thermal conduction mechanism. It is important to note that an exception was detected during the temperature increase with a unique rise in the semi-circle radius at 648 K. In order to analyze the impedance spectrum, it is useful to have an equivalent circuit model that provides a realistic representation of the electrical properties of the respective regions. Ideally, the semicircles can be modeled by a parallel RC element (Jiang et al., 2008; Song et al., 2005). In our case, the semicircles are depressed, thus in order to perform the fit of these curves, we have to replace the capacitance by a constant phase element (CPE) Liu et al., 2003. So, the equivalent circuit of $La_{1.85}Ca_{0.15}CuO_{3.5}$ sample can be modeled by a parallel connection of an ohmic resistor R_b and a CPE which are presented in Fig. S3. The total impedance will be given by:

$$Z^* = Z' + jZ'' = \left[\frac{1}{R_b} + \frac{1}{Z^*_{CPE}}\right]^{-1} \tag{9}$$

where Z' and Z'' are the real and the imaginary parts of the total impedance, respectively. The impedance of the CPE is defined via (Mulder et al., 1990; Komornicki et al., 2001; Friesen et al., 2000):

$$Z^*_{CPE} = [Q(j\omega)^{\alpha}]^{-1} \tag{10}$$

With ω the angular frequency ($\omega = 2\pi f$, f being the frequency) and j the imaginary unit ($j^2 = -1$), Q a constant independent of frequency and in F cm^2 $s^{\alpha-1}$ (Jorcin et al., 2006), and α the fractal exponent ranging between zero and unity. Moreover, Eq. (10) shows that if $\alpha \to 1$, $Z^*_{CPE} \to 1/jQ\omega$, involving a pure capacitance, whereas if $\alpha \to 0$, $Z^*_{CPE} \to 1/Q$, it behaves as a pure resistance. In order to determine the values of the parameters of the equivalent circuit which describes the compound $La_{1.85}Ca_{0.15}CuO_{3.5}$, the experimental data are simulated through the expressions (11) and (12).

$$Z' = \frac{R_b\left(1 + R_bQ\omega^{\alpha}\cos\left(\frac{\alpha\pi}{2}\right)\right)}{1 + 2R_bQ\omega^{\alpha}\cos\left(\frac{\alpha\pi}{2}\right) + (R_bQ\omega^{\alpha})}; \tag{11}$$

$$Z'' = \frac{R_b^2Q\omega^{\alpha}\sin\left(\frac{\alpha\pi}{2}\right)}{1 + 2R_bQ\omega^{\alpha}\cos\left(\frac{\alpha\pi}{2}\right) + (R_bQ\omega^{\alpha})^2} \tag{12}$$

Fig. 8 illustrates the variations of Z' and Z'' vs. frequency at 813 K of $La_{1.85}Ca_{0.15}CuO_{3.5}$ compound. The good agreement between the simulated and experimental data indicates that the proposed equivalent circuit describes well the electrical properties of the sample. The fit parameters at different temperature are listed in Table 5. It is observed that the Q variation with temperature presents two ranges of values [1.8–8.8 10^{-9} F cm^2 $s^{\alpha-1}$] before 648 K and [14.4–19.8 10^{-9} F cm^2 $s^{\alpha-1}$] after 648 K. The obtained theoretical Z' values are represented as a function of $-Z''$ values. The obtained curve is shown in the inset of Fig. 8 and presents a high conformity with the experimental Nyquist plot of the $La_{1.85}Ca_{0.15}CuO_{3.5}$ sample, insisting again on the validity of the chosen fit equivalent

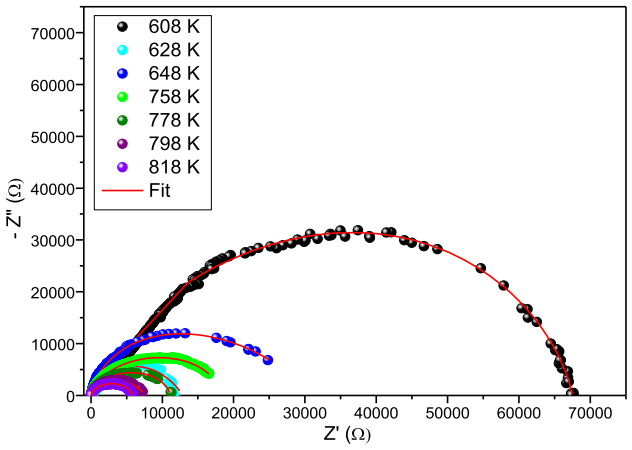

Figure 7 The Nyquist plots ($-Z''$ vs. Z') of impedance data at different temperatures for $La_{1.85}Ca_{0.15}CuO_{3.5}$ compound.

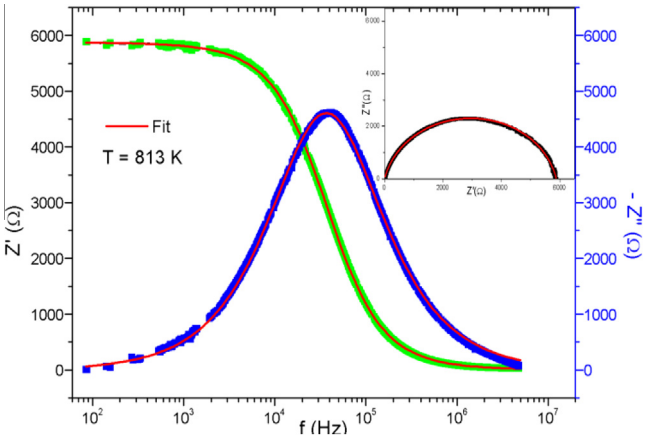

Figure 8 Variation of real and imaginary parts of impedance with frequency. Inset: Nyquist plots ($-Z''$ vs. Z') of impedance data at temperature $T = 813$ K for $La_{1.85}Ca_{0.15}CuO_{3.5}$ compound.

Table 5 The fitting values of equivalent circuit elements obtained at some temperatures.

T (K)	R_b (KΩ)	Q (10^{-9} F cm^2 s$^{\alpha-1}$)	α
608	67.540	1.823	0.899
628	12.820	8.812	0.840
648	29.295	1.836	0.936
758	18.475	14.435	0.857
778	11.170	16.685	0.860
798	7.393	17.407	0.861
818	5.778	19.841	0.858

circuit. The ac conductivity is determined from the data of complex impedance values and calculated at each temperature using the relation Pant et al. (2008):

$$\sigma_{ac} = (4e/\pi d^2)[Z'/(Z'^2 + Z''^2)] \quad (13)$$

The ac conductivity dependence on frequency (ω) at 813 K is shown in the inset of Fig. 9. At low frequencies, the ac conductivity is constant with frequency before making an abrupt increase at high frequencies. It is also observed that ac conductivity increases with temperature. The nature and mechanism of the conductivity dispersion in solids are described through Jonscher's universal power law expressed by:

$$\sigma_{ac} = \sigma_{dc} + A\omega^n \quad (14)$$

where σ_{dc} is the direct current conductivity, A is the temperature-dependent parameter that determines the strength of polarizability, n is the dimensional frequency exponent parameter in the range of $0 \leqslant n \leqslant 1$ (Lee et al., 1991; Palmer et al., 1984) representing the degree of interaction between mobile ions with the bound ions around them. Eq. (14) is referred to as the 'universal' dynamic pattern of the ac electrical behavior of conducting solids and liquids as proposed by Jonscher (1977). The anomaly observed at 640 K (367 °C) (Fig. 9) can be attributed to the phase transition (Pseudo-S → T′) manifested at 648 K as revealed by DSC measurements. Above 820 K, σ_{dc} decreases. This fact can be explained by the incremental oxidation of T′-phase at high temperature than the reversible tendency toward T-phase (see Fig. 1) as experimentally demonstrated by Houchati et al. (2012). The monitoring of the dc conductivity with temperature ($10^3/T$) presented in Fig. 10 shows an Arrhenius type behavior (Kim et al., 2003).

$$\sigma_{dc}T = \sigma_0 \exp\left(\frac{-E_a}{k_B T}\right) \quad (15)$$

where σ_0 is the pre-exponential factor which depends on a number of charge carriers and materials structural parameters, k_B is the Boltzmann constant and E_a is the activation energy. It can also be seen that the Log ($\sigma_{dc}T$) vs. ($10^3/T$) curves present two slopes, indicating that the conductivity is affected by two different transport mechanisms, each of which is predominating in a different temperature range. The two regions are indexed as I and II which are separated discontinuously at T = 648 K. This change in conductivity behavior was attributed to a phase transition (transition of the "pseudo–S" phase to the T′ phase) undergone by the compound. In fact, through the DSC measurement, this phase transition was clearly noted as demonstrated in Fig. S2. Actually, this notable change in the conductivity behavior was also observed with the Nyquist plots at T = 648 K and its fitting parameters. It should be noted that the electrodes were connected to the impedance meter using two contacts. Ideally, four contacts should be performed for a better accuracy (Errandonea et al., 2009). On the other hand, in spite that the use of two contacts will affect the absolute value of the conductivity, this will not affect remarkably their tendency and the slope of the results represented in Fig. 10, from which the activation energy is determined, is practically not influenced by this experimental detail. Therefore, the present results will lead to an accurate determination of the activation energy. The activation energy decreases from 0.9661 to 0.7614 eV when the structure passes from pseudo-S to T′ as shown in Fig. 10. Actually, the monitoring of the conductivity behavior of the T-phase was carried out in our previous work (Midouni et al., 2016). The study reveals that the parent phase presents an activation energy of 0.3748 eV.

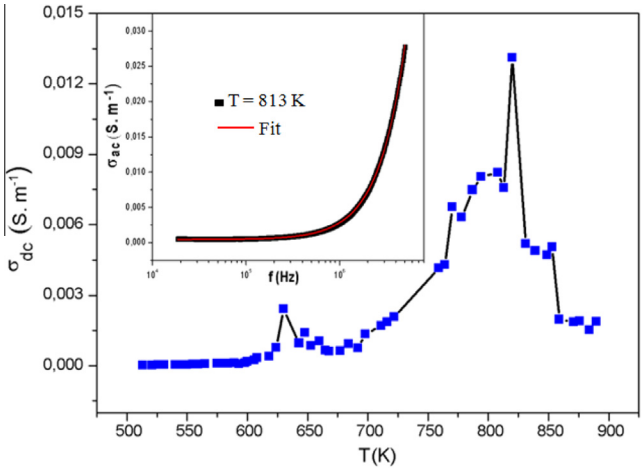

Figure 9 The frequency dependence of ac conductivity (σ_{ac}) at 813 K. The inset shows the variation of dc conductivity (σ_{dc}) a function of temperature for the $La_{1.85}Ca_{0.15}CuO_{3.5}$ system.

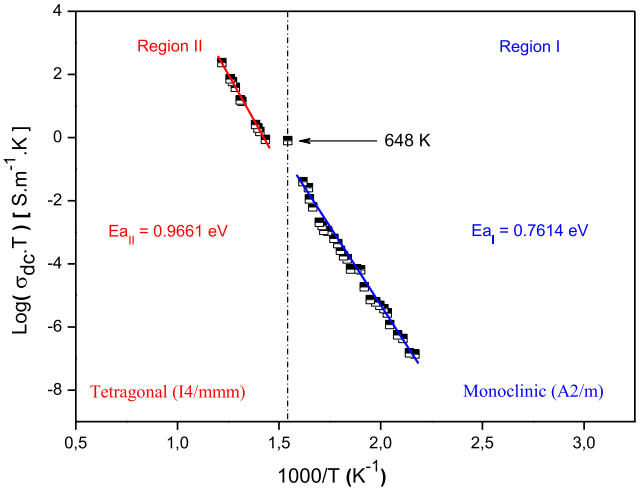

Figure 10 Arrhenius relation of Log (σ_{dc}·T) with the reciprocal of absolute temperature ($10^3/T$) for the $La_{1.85}Ca_{0.15}CuO_{3.5}$ compound.

Please cite this article in press as: Midouni, A. et al., Topochemical reduction of the oxygen-deficient Ruddlesden–Popper phase ($n = 1$) $La_{1.85}Ca_{0.15}CuO_{4-\delta}$ and electrical properties of the $La_{1.85}Ca_{0.15}CuO_{3.5}$. Arabian Journal of Chemistry (2016), http://dx.doi.org/10.1016/j.arabjc.2016.06.006

Passing to the reduced "pseudo-S" phase the activation energy increases to 0.7614 eV and then to 0.9661 eV with the T′-phase. This tendency highlights the role of oxygen sites distribution and symmetry in the conductivity process since this property is the most affected by the different phase transitions (see Fig. 1).

4. Conclusion

The present research work has confirmed that the low-temperature topochemical manipulation of complex oxides, either by reductive anion deintercalation or oxidative anion insertion, offers many opportunities for the rational synthesis of a wide range of new oxygen-ordered structures. The latter may be useful for solid oxide fuel cells, oxygen membranes and sensor materials oriented towards the reduction of working temperatures. During this work, the topotactic reduction of complex transition metal T-$La_{1.85}Ca_{0.15}CuO_{4-\delta}$ can lead to the preparation of novel anion-deficient phases with unique transition metal-oxygen $La_{1.85}Ca_{0.15}CuO_{3.5}$. The crystal structure of the mixed-valent Cu^{1+}/Cu^{3+} ($3d^{10}/3d^{8}$) phase belongs to the "pseudo-S" phase type. The electrical properties of the latter, $La_{1.85}Ca_{0.15}CuO_{3.5}$, was investigated by impedance spectroscopy as a function of temperature, revealing a consistent variation of electrical conductivity with phase transition. This behavior can be rationalized on the basis of the prevailing defect chemistry, involving oxygen vacancies. In fact, the variations of the elements values, which correspond to equivalent circuit with temperature, have confirmed the occurrence of the change in the conduction mechanism at 648 K detected by electric measurements.

Appendix A. Supplementary material

Supplementary data associated with this article can be found, in the online version, at http://dx.doi.org/10.1016/j.arabjc.2016.06.006.

References

Alyoshin, V.A., Romanova, I.P., Mikhailova, D., Oswald, S., Senyshyn, A., Ehrenberg, H., 2010. J. Phys. Chem. A 114, 13362.
Bouloux, J.C., Soubeyroux, J.L., Daoudi, A., Flem, G.L., 1981. Mater. Res. Bull. 16, 855.
Chou, F.C., Cho, J.H., Miller, L.L., Johnston, D.C.J., 1990. Phys. Rev. B 42, 6172.
Dixon, E., Hayward, M.A., 2011. Inorg. Chem. 50, 7250.
Dixon, E., Hadermann, J., Ramos, S., Goodwin, A.L., Hayward, M. A.J., 2011. Am. Chem. Soc. 133, 18397.
Errandonea, D., Segura, A., Martínez-García, D., Muñoz-San Jose, V., 2009. Phys. Rev. B 79, 125203.
Friesen, G., Ozsar, M.E., Dunlop, E., 2000. Thin Solid Films 361–362, 303.
Grimnes, S., Martinsen, O.G., 2005. IEEE Eng. Med. Biol. Soc. 52, 132.
Hayward, M.A., 2005. Chem. Mater. 17, 670.
Hayward, M.A., 2006. Chem. Mater. 18, 321.
Hayward, M.A., Rosseinsky, M.J., 2000. Chem. Mater. 12, 2182.
Hayward, M.A., Green, M.A., Rosseinsky, M.J., Sloan, J., 1999. J. Am. Chem. Soc. 121, 8843.
Houchati, M.I., Ceretti, M., Ritter, C., Paulus, W.J., 2012. Chem. Mater. 24, 3811.
Houchati, M.I., Houchati, I., Midouni, A., Ceretti, M., Hamzaoui, A. H., Paulus, W., 2014. Arab. J. Chem.
Jiang, J., Zhang, T.J., Zhang, B.S., Mao, H., 2008. J. Electroceram. 21, 258.
Jonscher, A.K., 1977. Nature 267, 673.
Jorcin, J.B., Orazem, M.E., Pébére, N., Tribollet, B., 2006. Electrochim. Acta. 51, 1473.
Kageyama, H., Watanabe, T., Tsujimoto, Y., Kitada, A., Sumida, Y., Kanamori, K., Yoshimura, K., Hayashi, N., Muranaka, S., Takano, M., Ceretti, M., Paulus, W., Ritter, C., André, G., 2008. Angew. Chem., Int. Ed. 47, 5740.
Kim, J.E., Kim, S.J., Choi, H.W., Yang, Y.S., 2003. J. Korean Phys. Soc. 42, 1224.
Komornicki, S., Radecka, M., Rekas, M., 2001. J. Mater. Sci. 12, 11.
Krogh Andersen, I.G., Krogh Andersen, E., Norby, P., Skou, E., 1994. J. Solid State Chem. 113, 320.
Laligant, Y., Bail, L.A., Ferey, G., Hervieu, M., Raveau, B., Wilkinson, A., Cheetham, K.A., 1988. Synthesis and Ab-Initio Structure Determination from X-ray Powder Data of Ba[2]PdO[3] with SevenfoldCoordinated Ba[2+]. Structural Correlations with K[2]NiFu and Ba[2]NiF[6]; Gauthier-Villars: Paris, France, Vol. 25.
Lee, W.K., Liu, J.F., Nowick, A.S., 1991. Phys. Rev. Lett. 67, 1559.
Liu, J., Duan, C.G., Yin, W.G., Mei, W.N., Smith, R.W., Hardy, J.R., 2003. J. Chem. Phys. 119, 2812.
McCusker, L.B., R.B.V. D., Cox, D.E., Louer, D., Scardie, P.J., 1999. Appl. Crystallogr. 32, 36.
Midouni, A., Houchati, M.I., Belhaj Othman, W., Chniba-Boudjada, N., Jaouadi, M., Ceretti, M., Paulus, W., Hamzaoui, A.H., 2016. J. Solid State Chem. 240, 101.
Mohn, C.E.S.S., Norberg, S.T., Hull, S., 2009. Phys. Rev. Lett. 102, 155502.
Mulder, W.H., Sluyters, J.H., Pajkossey, T., Nyikos, L.J., 1990. Electro-Anal. Chem. 285, 103.
Palmer, R.G., Stein, D.L., Abrahams, E., Anderson, P.W., 1984. Phys. Rev. Lett. 53, 958.
Pant, M., Kanchan, D.K., Sharma, P., Jayswal, M.S., 2008. Mater. Sci. Eng. B 149, 18.
Pederzolli, D.R., Attfield, J.P., 1998. J. Solid State Chem. 136, 137.
Pokrovsky, V.L., Uimin, G.V., 1989. Physica C 160, 323.
Poltavets, V.V., Lokshin, K.A., Dikmen, S., Croft, M., Egami, T., Greenblatt, M.J., 2006. Am. Chem. Soc. 128, 9050.
Rietveld, H., 1969. J. Appl. Crystallogr. 2, 65.
Rodríguez-Carvajal, 1993. J. Phys. B 192, 55.
Ruiz-Fuertes, J., Friedrich, A., Pellicer-Porres, J., Errandonea, D., Segura, A., Morgenroth, W., Haussühl, E., Tu, C.-Y., Polian, A.J., 2011. Chem. Mater. 23, 4220.
Sai Sundar, V.V.S.S., Karthikeyani, A., Jagannathan, R., 1999. J. Chem. Phys. Lett. 301, 417.
Seddon, J., Suard, E., Hayward, M.A., 2010. J. Am. Chem. Soc. 132, 2802.
Song, S.G., Ling, Z., Placido, F., 2005. Mater. Res. Bull. 40, 1081.
Stolen, S., Mohn, C.E., Ravindran, P., Allan, N.L., 2005. J. Phys. Chem. B 109, 12362.
Tassel, C., Watanabe, T., Tsujimoto, Y., Hayashi, N., Kitada, A., Sumida, Y., Yamamoto, T., Kageyama, H., Takano, M., Yoshimura, K., 2008. J. Am. Chem. Soc. 130, 3764.
Tassel, C., Pruneda, J.M., Hayashi, N., Watanabe, T., Kitada, A., Tsujimoto, Y., Kageyama, H., Yoshimura, K., Takano, M., Nishi, M., Ohoyama, K., Mizumaki, M., Kawamura, N., Iniguez, J., Canadell, E., 2009. J. Am. Chem. Soc. 131, 221.
Tassel, C., Seinberg, L., Hayashi, N., Ganesanpotti, S., Ajiro, Y., Kobayashi, Y., Kageyama, H., 2013. Inorg. Chem. 52, 6096.
Teske, C.L., Müller-Buschbaum, H., 1969a. Z. Anorg. Allg. Chem. 370, 134.
Teske, C.L., Müller-Buschbaum, H., 1969b. Z. Anorg. Allg. Chem. 371, 325.
Trigui, W., Oueslati, A., Chaabane, I., Hlel, F., 2015. J. Solid State Chem. 227, 10.
Tsujimoto, Y., Tassel, C., Hayashi, N., Watanabe, T., Kageyama, H., Yoshimura, K., Takano, M., Ceretti, M., Ritter, C., Paulus, W., 2007. Nature 450, 1062.

Please cite this article in press as: Midouni, A. et al., Topochemical reduction of the oxygen-deficient Ruddlesden–Popper phase ($n = 1$) $La_{1.85}Ca_{0.15}CuO_{4-\delta}$ and electrical properties of the $La_{1.85}Ca_{0.15}CuO_{3.5}$. Arabian Journal of Chemistry (2016), http://dx.doi.org/10.1016/j.arabjc.2016.06.006

Wasel-Nielen, H.D., Hoppe, R., 1970. Z. Anorg. Allg. Chem. 375, 209.
Wong-Ng, W.K., Davis, K.L., Roth, R.S., 1988. J. Am. Ceram. Soc., 71
Yamamoto, T., Li, Z., Tassel, C., Hayashi, N., Takano, M., Isobe, M., Ueda, Y., Ohoyama, K., Yoshimura, K., Kobayashi, Y., Kageyama, H., 2010. Inorg. Chem. 49, 5957.
ZView for Windows, Impedance/Gain Phase Graphing and Analysis Software; Scribner Associates Inc: Southern Pines, NC.

Please cite this article in press as: Midouni, A. et al., Topochemical reduction of the oxygen-deficient Ruddlesden–Popper phase ($n = 1$) $La_{1.85}Ca_{0.15}CuO_{4-\delta}$ and electrical properties of the $La_{1.85}Ca_{0.15}CuO_{3.5}$. Arabian Journal of Chemistry (2016), http://dx.doi.org/10.1016/j.arabjc.2016.06.006